Expression of mRNA encoding the H1, H2, and H3 histamine receptors in the rat cochlea

Hiroshi Azuma,[CA] Shoichi Sawada, Shunji Takeuchi, Kasumi Higashiyama, Akinobu Kakigi and Taizo Takeda

Department of Otolaryngology, Kochi Medical School, Nankoku, Kochi, 783-8505, Japan

[CA]Corresponding Author: azuma@kochi-ms.ac.jp

Received 25 November 2002; accepted 2 January 2003

DOI: 10.1097/01.wnr.0000058956.85541.7e

Histamine may have physiological functions in the inner ear. Histamine receptors, however, have not yet been identified in the mammalian cochlea. We determined, using reverse transcription polymerase chain reaction (RT-PCR), that H1, H2, and H3 histamine receptor mRNA is expressed in the rat cochlea. To investigate the distribution of each receptor, the cochlea was divided into three parts: the lateral portion, the medial portion, and the modiolus. The mRNA for each receptor subtype was detected in the modiolus but not in the lateral and medial portions of the cochlea. This is the first evidence of H1, H2, and H3 histamine receptor mRNA in the rat cochlea. These findings support the suggestion that histamine may play a physiological role in the cochlea. *NeuroReport* 14:423–425 © 2003 Lippincott Williams & Wilkins.

Key words: Cochlea; Histamine receptor; mRNA; Neurotransmitter; RT-PCR

INTRODUCTION

Histamine influences diverse physiological processes in many types of cells through histamine receptors classified as H1, H2, and H3 receptors [1]. The histamine receptor subtypes are members of the superfamily of G-protein-coupled receptors and each subtype (H1, H2, and H3) has been cloned recently [2–4]. Histamine H1 receptor stimulation causes contraction of tracheal and vascular smooth muscles, increases vascular permeability, and excites sensory nerve endings. The histamine H2 receptor mediates gastric acid secretion and relaxation of airway and vascular smooth muscles [5]. Histamine H3 receptor stimulation inhibits the synthesis and release of histamine itself [6]. In the brain, histamine is synthesized in histaminergic neurons and acts as a neurotransmitter and/or modulator [7,8]. The cell bodies of these neurons are localized in the tuberomammillary nucleus of the hypothalamus, and their axons are widely distributed in various areas of the brain and spinal cord [9,10].

Potential physiological functions of histamine in the mammalian cochlea [11,12] have been proposed; however, histaminergic innervation and/or histamine receptor expression have not so far been described in the cochlea. Our aim in this study was to elucidate the expression pattern of histamine receptor mRNA in the rat cochlea using RT-PCR.

MATERIALS AND METHODS

Animals and preparation of specimens: Twelve healthy female Wistar rats (200–280 g) were deeply anesthetized with pentobarbital sodium (100 mg/kg, i.p.) and perfused with a solution (NaCl 110 mmol/l, Na aspartate 40 mmol/l, KCl 3.6 mmol/l, $MgCl_2$ 1 mmol/l, HEPES 6 mmol/l, glucose 5 mmol/l, pH 7.4) via the left ventricle to wash out the blood. First, the cochleae and brains from three animals were dissected under a stereomicroscope. In order to investigate receptor mRNA distribution in the cochlea, cochleae from three other animals were dissected under a stereomicroscope and divided into three portions: the lateral portion, including the spiral ligament and the stria vascularis, the medial portion, including the organ of Corti, and the modiolus. This study was approved by the Kochi Medical School Animal Care and Use Committee, which conformed to The Animal Welfare Act and the guiding principles for animal care developed by the Ministry of Education, Culture, Sports and Technology, Japan.

Isolation of total RNA and removal of genomic DNA from total RNA samples: Total RNA was extracted from each tissue using the RNeasy Mini Kit (Qiagen, Hilden, Germany). In order to eliminate residual genomic DNA that might produce a false positive amplification signal, we added on-column DNase digestion with the RNase-free DNase set (Qiagen, Hilden, Germany).

RT-PCR: cDNA was synthesized from total RNA by reverse transcription (SuperScriptII kit, Promega, Madison, WI, USA). PCR was performed using HotStar Taq (Qiagen, Hilden, Germany). Each PCR reaction was carried out using

Table I. Primer sequences to for the histamine receptors.

		Prime sequence	Length of PCR product (bp)
H1 receptor	Sense	5′-CTTCTACCTCCCCACTTTGCT-3′	292
	Antisense	5′-TTCCCTTTCCCCCTCTTG-3′	
H2 receptor	Sense	5′-TTCTTGGACTCCTGGTGCTGC-3′	309
	Antisense	5′-CATGCCCCCTCTGGTCCC-3′	
H3 receptor	Sense	5′-CCAGAACCCCCACCAGATG-3′	297 (H3S)
	Antisense	5′-CCAGCAGAGCCCAAAGATG-3′	393 (H3L)

specific oligonucleotide primers based on the published sequences of the rat H1 receptor (GenBank, AF387889), H2 receptor (GenBank, NM012965), H3-L receptor (GenBank, AY009370), and H3-S receptor (GenBank, AY009371). The sequences of the primers and the expected band sizes are shown in Table 1. PCR was carried out using a thermal cycler (TP3000, Takara, Otsu, Shiga, Japan) with an initial denaturing period of 15 min at 95°C, followed by 35 cycles at 94°C for 1 min, 58°C for 1 min, 72°C for 1 min and a final extension period of 10 min at 72°C. PCR amplified products (10 µl) were electrophoresed on 3% agalose gel and stained with ethidium bromide. The PCR products were sequenced directly using ABI PRISM 310 with the BigDye terminator cycle sequencing kit (PE Applied Biosystems, Foster City, CA, USA).

RESULTS

RT-PCR analysis revealed that H1 and H2 receptor mRNAs are expressed in the rat cochlea and brain (Fig. 1). PCR products obtained from these tissues were of the expected size (H1: 294 bp, H2: 309 bp). Each nucleotide sequence of the PCR products agreed completely with the known sequences (H1: GenBank AF387889, H2: NM012965). The H3 receptor PCR product was represented by two bands (Fig. 1). We sequenced both bands after separating them from an agarose gel. The nucleotide sequence of the larger mol. wt band matched the H3L sequence exactly (393 bp, GenBank AY009370) and the sequence of the smaller mol. wt band matched the H3S sequence (251 bp, GenBank AY009371). H3L and H3S are isoforms of the H3 receptor. These PCR products were not obtained when RT was omitted (Fig. 1, negative controls), indicating that the PCR products were derived from mRNA, not from genomic DNA. mRNA for the histamine receptors (H1, H2, and H3 receptors) could be detected in the modiolus, but not in the medial and lateral portions of the cochlea (Fig. 2).

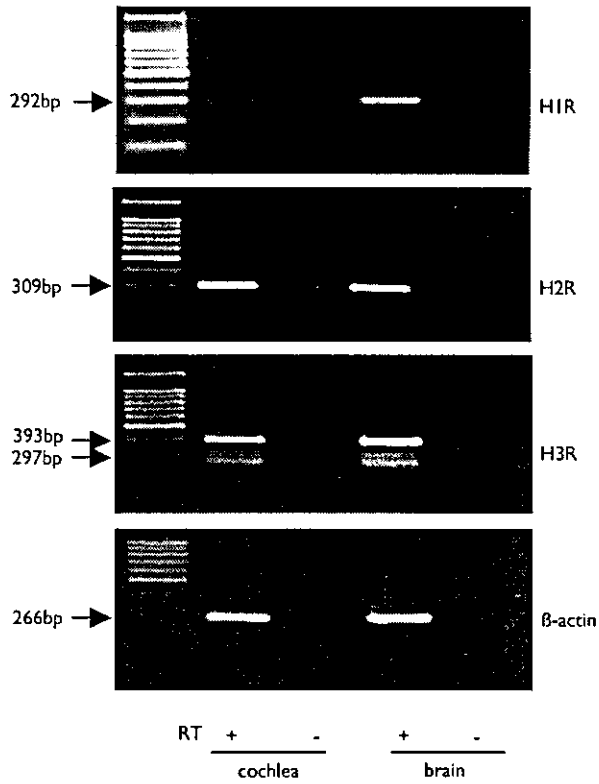

Fig. 1. RT-PCR products with the specific primer pairs of the H1, H2, and H3 receptors were electrophoresed on a 3% agarose gel. cDNA from the rat cochlea and brain was amplified by PCR in 35 cycles. Arrows indicate histamine H1 receptor (H1R, 292 bp), H2 receptor (H2R, 309 bp), H3 receptor (H3L, 393 bp; H3S, 297 bp). RT (+): with reverse transcription; RT (−): without reverse transcription for negative control.

DISCUSSION

Physiological functions of histamine in the inner ear have been suggested in several reports but not firmly established. Results from electrophysiological studies on the equilibrium organ of frogs have suggested that histamine acts as a hair cell transmitter [13–15]. Only two electrophysiological studies examining histamine in the mammalian cochlea have been reported [11,12]. Infusion of 10 mM histamine into the scala tympani of guinea pigs demonstrated only a slight decrease in the compound action potential amplitude [11]. Minoda *et al.* [12] reported that infusion of 10–50 µM histamine solutions into the scala tympani increased the compound action potential amplitude, while infusion of a 10 mM solution decreased the amplitude. Thus, they speculated that histamine at a low concentration might act as a neurotransmitter or neuromodulator. Previous studies have suggested that histamine may play a physiological role in the inner ear but histamine receptor expression has not been reported previously.

In this study, we have found that mRNAs encoding the H1, H2, and H3 histamine receptors are expressed in the modiolus of the rat cochlea. The major components of the modiolus, which is the axial part of the cochlea, are the spiral ganglion, nerve fibers, cochlear artery and cochlear vein. In the brain, histamine is synthesized in histaminergic

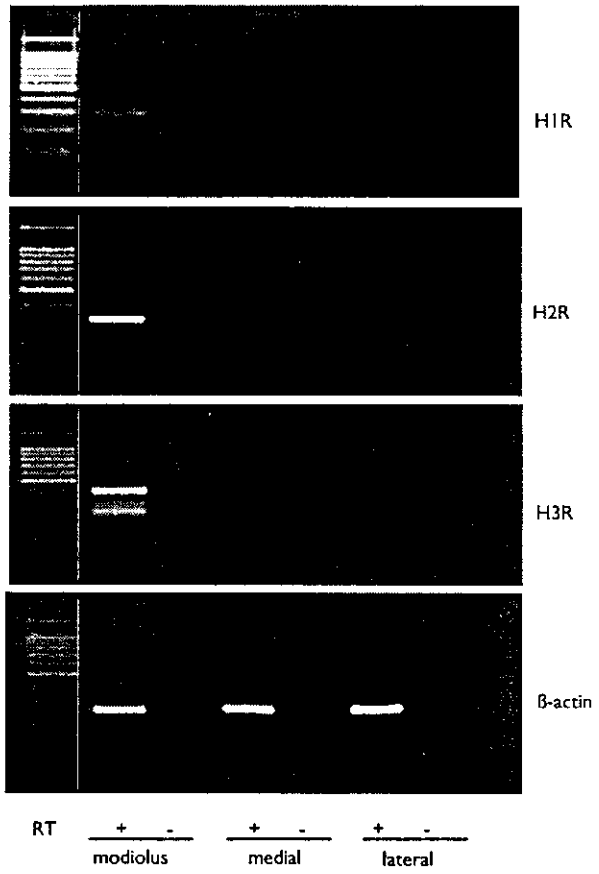

Fig. 2. RT-PCR products from the modiolus, the medial portion, and the lateral portion were electrophoresed on a 3% agarose gel. Only the modiolus showed the specific bands for the H1, H2, and H3 receptors. The sequences of the two bands for the H3 receptor match the H3L (393 bp) and H3S (297 bp) isoforms. RT (+): with reverse transcription; RT (−): without reverse transcription for negative control.

neurons and acts as a transmitter and/or modulator. Activation of the H1 receptor induces a mobilization of Ca^{2+} and activation of the H2 receptor causes an increase in the cAMP level [16]. The H1 and H2 receptors, expressed in vascular smooth muscle, contribute to vascular contraction and dilation [5]. Our measured expression of H1 and H2 receptor mRNA may indicate localization of these receptors in the cochlear artery. Furthermore, our finding that H3 receptor mRNA is expressed in the modiolus suggests that there may be histaminergic innervation in the cochlea. Histamine receptors are widely expressed in the brain and are thought to be important in neuronally mediated functions such as arousal and anxiety, and in the activation of the sympathetic nervous system [16]. Additional physiological studies are now needed to clarify the functions of histamine in the cochlea.

CONCLUSION

H1, H2, and H3 histamine receptor mRNA is expressed in the rat cochlea via RT-PCR. All three receptor subtypes were expressed in the modiolus of the cochlea. This is the first evidence of H1, H2, and H3 histamine receptor mRNA in the rat cochlea. These findings support the suggestion that histamine may play a physiological role in the cochlea.

REFERENCES

1. Arrang JM. *Cell Mol Biol* **40**, 273–279 (1994).
2. Yamashita M, Fukui H, Sugama K *et al. Proc Natl Acad Sci USA* **88**, 11515–11519 (1991).
3. Gantz I, Schaffer M, Delvalle J *et al. Proc Natl Acad Sci USA* **88**, 429–433 (1991).
4. Lovenberg TW, Roland BL, Wilson SJ *et al. Mol Pharmacol* **55**, 1101–1107 (1999).
5. Hill SJ. *Pharmacol Rev* **42**, 45–83 (1990).
6. Arrang JM, Garbarg M, Schwartz JC. *Nature* **302**, 832–837 (1983).
7. Schwartz JC, Arrang JM, Garbarg H *et al. Physiol Rev* **71**, 1–51 (1991).
8. Wada H, Inagaki N, Yamatodani A *et al. Trends Neurosci* **14**, 415–418 (1994).
9. Panula P, Yang HY and Costa E. *Proc Natl Acad Sci USA* **81**, 2572–2576 (1984).
10. Watanabe T, Taguchi Y, Shiosaka S *et al. Brain Res* **295**, 13–25 (1984).
11. Bobbin RP and Thompson MH. *Ann Otol Rhinol Laryngol* **87**,185–190 (1978).
12. Minoda R, Toriya T, Masuyama K *et al. Auris Nasus Larynx* **28**, 219–222 (2001).
13. Norris CH, Guth PS and Quine DB. *Proc Annu Meet Ass Res Otolaryngol*, 10th Clearwater Beach FL, p. 102 (1987).
14. Housley GD, Norris CH and Guth PS. *Hear Res* **35**, 87–98 (1998).
15. Bledsoe SC Jr, Sinard RJ and Allen SJ. *Hear Res* **38**, 81–93 (1989).
16. Brown RE, Stevens DR and Haas HL. *Prog Neurobiol* **63**, 637–672 (2001).

Acknowledgements: This study was supported by a Grant-in-Aid for Scientific Research (C) from The Ministry of Education, Culture, Sports, Science and Technology, Japan (12671671).

Available online at www.sciencedirect.com
SCIENCE DIRECT
Hearing Research 181 (2003) 15–19
HEARING RESEARCH
www.elsevier.com/locate/heares

Aquaporin-1 (AQP1) is expressed in the stria vascularis of rat cochlea

Shoichi Sawada [a,*], Taizo Takeda [a], Hiroya Kitano [b], Shunji Takeuchi [a], Teruhiko Okada [c], Motonori Ando [d], Mikio Suzuki [b], Akinobu Kakigi [a]

[a] *Department of Otolaryngology, Kochi Medical School, Nankoku, Kochi 783-8505, Japan*
[b] *Department of Otolaryngology, Shiga University of Medicine, Otsu, Shiga, Japan*
[c] *Department of Anatomy, Kochi Medical School, Nankoku, Kochi, Japan*
[d] *Department of Physiology, Kochi Medical School, Nankoku, Kochi, Japan*

Received 19 November 2001; accepted 13 January 2003

Abstract

Cochlea endolymph, produced by the stria vascularis, is essential for normal inner ear function. Abnormal endolymphatic volumes correlate closely with pathological conditions such as Ménière's disease. The critical roles played by aquaporins, which facilitate osmotic movement of water molecules, are known in a variety of tissues. We investigated the expression of aquaporin-1 (AQP1) in the rat inner ear using reverse transcription polymerase chain reaction and immunohistochemical methods. We obtained novel data showing that not just AQP1 mRNA but also AQP1 protein is expressed in the stria vascularis, in addition to other data confirming previous reports. AQP1 immunoreactivity localized to the intermediate cells in the stria vascularis. The above finding suggests that AQP1 may play a role in the water distribution associated with vigorous ion transport in the stria vascularis since the intermediate part of the stria vascularis contains both intermediate cells and the basolateral parts of marginal cells, both of which express ion transporters abundantly.

Key words: Endolymph; Water transport; Polymerase chain reaction; Immunohistochemistry

1. Introduction

Endolymph is confined within a closed space, and an abnormal endolymph volume correlates closely with pathophysiological conditions of the inner ear. For example, an abnormal increase in endolymph volume, known as endolymphatic hydrops, occurs in Ménière's disease (Hallpike and Cairns, 1938). In Ménière's disease, disorders of the mechanisms underlying fluid homeostasis have been suggested (Bagger-Sjöbäck, 1999). It is generally accepted that endolymph in the cochlea is produced by the stria vascularis, a major component of the lateral wall of the cochlear duct. The endolymphatic sac, an extension of the endolymphatic space, may absorb endolymph and regulate the endomorph volume (Bagger-Sjöbäck, 1999; Kimura, 1967). In spite of the importance of inner ear fluid homeostasis, mechanisms underlying the volume control are still obscure.

Aquaporin-1 (AQP1), originally cloned from erythrocytes (van Os et al., 2000), is expressed in a variety of tissues, including renal tubular epithelial cells and the choroid plexus (Denker et al., 1988). Osmotic water permeability of renal proximal tubules and active water reabsorption were substantially reduced in AQP1-knockout mice (Schnermann et al., 1998). In the inner ear, it has been reported that AQP1 mRNA is expressed in the organ of Corti's, stria vascularis, vestibule, Reissner's membrane, and endolymphatic sac (Beitz et al., 1999). In addition, an immunohistochemical study has shown AQP1 immunoreactivity in type III fibrocytes of the spiral ligament, spiral limbus, and cells under the basilar membrane (Stankovic et al., 1995; Takumi et al., 1998). With regard to the expression of AQP1 in the stria vascularis, there is a discrepancy between a positive result at the mRNA level (Beitz

* Corresponding author. Tel.: +81 (88) 880-2393; Fax: +81 (88) 880-2395.
E-mail address: sawadas@kochi-ms.ac.jp (S. Sawada).

0378-5955/03/$ – see front matter © 2003 Elsevier Science B.V. All rights reserved.
doi:10.1016/S0378-5955(03)00131-X

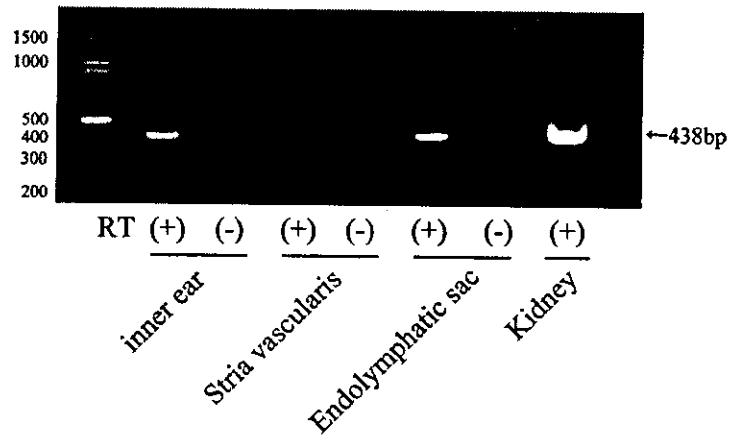

Fig. 1. RT-PCR analysis of AQP1 expression in the rat inner ear. RT-PCR products were electrophoresed on 3% agarose gels. RT (+): templates with reverse transcription, RT (−): templates with no reverse transcription as negative controls. The bands of all templates (the inner ear, the stria vascularis, the endolymphatic sac and the kidney) with reverse transcription showed the expected size of 438 bp. The sequence of all RT-PCR products was exactly the same as the known sequence of rat AQP1 cDNA.

et al., 1999) and a negative result at the protein level (Stankovic et al., 1995) as mentioned above. This study reports the expression of both mRNA and protein of AQP1 in the stria vascularis via reverse transcription polymerase chain reaction (RT-PCR) and histochemistry including immunoelectron microscopy.

2. Materials and methods

2.1. Subjects

Twenty healthy Wistar rats (200–300 g) were used. The animal protocols of this study were approved by the Animal Care Committee of the Kochi Medical School.

2.2. RT-PCR

Animals were deeply anesthetized with sodium pentobarbital (100 mg/kg, i.p.) and perfused with phosphate-buffered saline (PBS, 10 mM phosphate buffer salts, 137 mM NaCl, 2.7 mM KCl) (pH 7.4) from the left ventricle to remove blood. Tissue specimens were then dissected under a microscope. mRNA was prepared from three kinds of inner ear tissues (the whole inner ear, the stria vascularis and the endolymphatic sac) and from kidney, for use as a positive control. Two inner ears were used to obtain mRNA for each of the whole inner ear, the stria vascularis, and the endolymphatic sac. Tissue strips of the stria vascularis were separated from the underlying spiral ligament (Takeuchi et al., 1995). The specimen of the endolymphatic sac was separated from the vestibular aqueduct carefully while it was difficult to completely remove connective tissue from around the endolymphatic sac. mRNA was purified using the QuickPrep Micro mRNA purification kit (Pharmacia, Piscataway, NJ, USA). RT-PCR was performed using the SuperScriptII kit (Promega, Madison, WI, USA) and a thermal cycler (TP3000, Takara, Otsu, Shiga, Japan). The primers used for detection of specific cDNA were 5′-CGTCTTCATCAGCATCGGTTCT-3′ (sense) and 5′-CAGTGGTAGCCAGAACGCACAG-3′ (antisense) for rat AQP1 (GenBank accession number NM_012778). After preincubation for 10 min at 94°C, RT-PCR was performed for 1 min at 94°C, 1 min at 55°C, and 1 min at 72°C, and repeated for 35 cycles. RT-PCR products were sep-

→

Fig. 2. Immunostaining of the rat inner ear for AQP1, visualized by the diaminobenzidine tetrahydrochloride method (in brown). Nuclei were stained with hematoxylin. (A) Low power view of the cochlea. The stria vascularis (open arrowheads) and cells in the spiral ligament close to the bony wall (filled arrowheads) show strong immunoreactivity. Cells lining the perilymphatic surface of the scala vestibuli (open arrows) and the scala tympani (filled arrows) were weakly stained. Scale bar, 100 μm. (B) Magnified view of the stria vascularis. Open arrowheads, the stria vascularis. Filled arrowheads, cells in the spiral ligament close to the bony wall. Scale bar, 10 μm. (C) Negative control. This section was processed in the same way as B except for pre-adsorption of the primary antibody by control peptide. Scale bar, 10 μm. (D) Low power view of vestibule. Periosteum and fibrocytes in connective tissue were stained. c, basal turn of the cochlea; n, vestibular nerve; s, saccule; u, utricle. Scale bar, 200 μm. (E) Magnified view of the rectangular area in D, showing saccular epithelial cells and underlying connective tissue. Immunoreactivity was not detected in the saccular epithelial cells. Scale bar, 10 μm. (F) Low power view of endolymphatic sac. cc, common crus; es, endolymphatic sac; ss, sigmoid sinus. Scale bar, 200 μm. (G) Magnified view of the rectangular area in F. Abbreviations are the same as in F. Immunoreactivity was observed in the connective tissue around the endolymphatic sac but not in the epithelial cells in the endolymphatic sac. Scale bar, 10 μm.

arated on 3% agarose gels, and stained with ethidium bromide.

2.3. Sequencing of PCR products

RT-PCR products were purified with the Wizard PCR Preps DNA Purification System (Promega). The purified PCR product solution (2 μl) was mixed with Terminator Ready Reaction Mix (16 μl) and 10 pmol of sense or antisense primer, and then PCR was performed for 30 s at 96°C, 15 s at 50°C and 4 min at 60°C, and repeated for 25 cycles on the thermal cycler (TP3000,

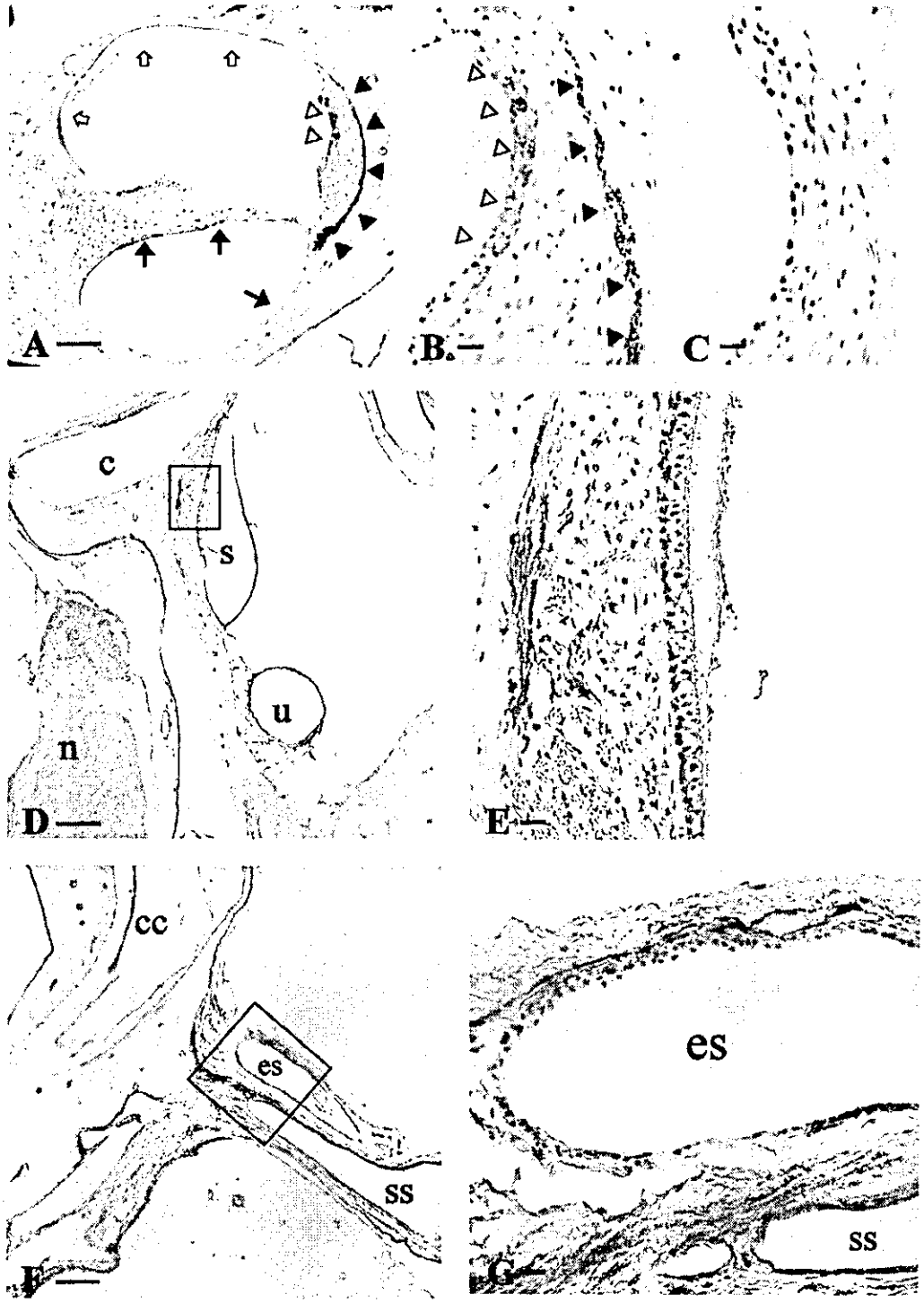

Takara). The products were re-purified by Centri Spin Column (Princeton Separation, Adelphia, NJ, USA). Purified products were mixed with a template suppression reagent (PE Applied Biosystems, Foster City, CA, USA), dried with a vacuum centrifuge, and then sequenced with ABI Prism 310 Genetic Analyzer (PE Applied Biosystems).

2.4. Immunohistochemistry

Animals were anesthetized by the same method as mentioned above and perfused from the left ventricle with PBS, followed by a fixative (pH 7.4) containing 4% paraformaldehyde in PBS. Temporal bones were dissected and immersed in the fixative overnight, and then decalcified in 0.12 M ethylenediamine tetraacetic acid in PBS (pH 7.4) for 21 days. Decalcified temporal bones were dehydrated in a series of graded concentrations of ethanol and embedded in paraffin. Sections (5 μm thick) were deparaffinized and immersed in 100% methanol with 3% hydrogen peroxide for 15 min to block endogenous peroxidase activity. Sections were incubated for 10 min in normal goat serum (Histofine SAB kit, Nichirei, Tokyo, Japan) and exposed to the primary antibody (diluted 1:1000), for 3 h at room temperature. The primary antibody (#AB3065, Chemicon, Temecula, CA, USA) was raised in rabbits against a synthetic peptide corresponding to the carboxy-terminal domain (amino acids 251–269) of rat AQP1 and affinity-purified. Sections were exposed to secondary antibody (anti-rabbit IgG, Histofine SAB kit) conjugated with biotin, and then to streptavidin conjugated with peroxidase. The sections were incubated with diaminobenzidine solution (1 ml of Tris–HCl buffer; 50 μl of 0.03 M 3,3′-diaminobenzidine·4HCl solution; 50 μl of 0.6% H_2O_2 solution) for 5 min and washed with distilled water. Hematoxylin was used for counterstain. A negative control study was performed using the AQP1 peptide comprised of 19 amino acids (#752P, Alpha Diagnostic, San Antonio, TX, USA). The primary antibody was pre-adsorbed by the AQP1 peptide for 30 min at 37°C, and then centrifuged for 10 min at 3000 rpm. The supernatant was used in place of the primary antibody as in the above-mentioned protocol.

2.5. Immunoelectron microscopy

Ultrathin sections were made as reported previously (Takeuchi et al., 1995). Sections were immersed in 0.3% H_2O_2 for 5 min and then in 1% bovine serum albumin. They were incubated with the same antibody (1:1000) at 4°C overnight. After a rinse with PBS, they were incubated with goat anti-rabbit IgG–15 nm colloidal gold conjugate (Funakoshi, Tokyo, Japan) for 60 min at room temperature. The sections were washed with PBS and stained with uranyl acetate and lead citrate.

3. Results and discussion

RT-PCR of micro-dissected tissues revealed that AQP1 mRNA was expressed in the stria vascularis

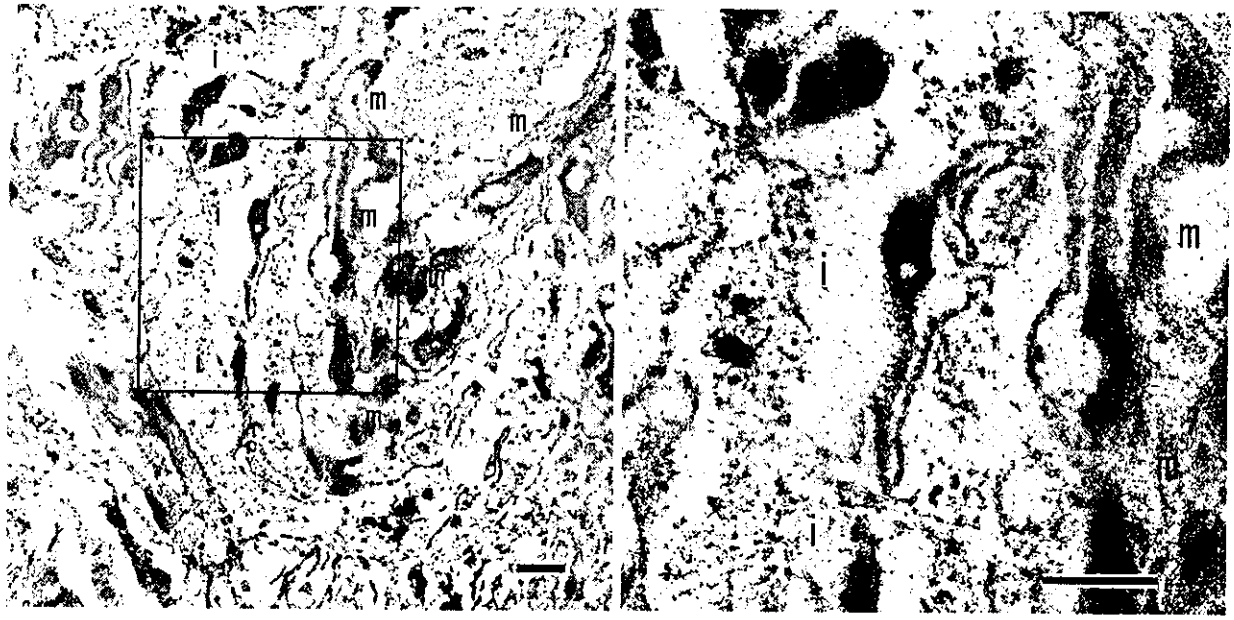

Fig. 3. Immunoelectron microscopy of the rat stria vascularis for AQP1, visualized by the colloidal gold conjugate (15 nm). The immunolabeled gold was seen in the intermediate cells of the stria vascularis. m, marginal cell; i, intermediate cell. (A) Low power view. Scale bar, 10 μm. (B) Magnified view of the rectangular area in A. Scale bar, 10 μm.

and in the endolymphatic sac (Fig. 1). The RT-PCR products were the expected size of 438 bp and the nucleotide sequence of the bands agreed exactly with the known sequence of rat AQP1 (GenBank accession number NM_012778). These results confirmed a previous RT-PCR study (Beitz et al., 1999). In the histochemical studies, relatively strong AQP1 immunoreactivity was observed in the stria vascularis and cells in the spiral ligament close to the bony wall (Fig. 2A,B), and weaker immunoreactivity in cells lining the perilymphatic surface of the scala vestibuli and the scala tympani (Fig. 2A). These results agreed with a previous report (Stankovic et al., 1995) except for our positive result in the stria vascularis. Positive immunoreactivity could be considered to be specific to the peptide of AQP1 since the immunoreactivity disappeared when the primary antibody was pre-absorbed by the antigenic peptide (Fig. 2C). Our results resolved the discrepancy between previous reports with regard to the expression of AQP1 in the stria vascularis, i.e. a positive result at the mRNA level (Beitz et al., 1999) and a negative result at the protein level (Stankovic et al., 1995). We speculated that the difference in the animal species and/or the primary antibody employed might caused the difference between the previous report (Stankovic et al., 1995) and this study. Immunoelectron microscopy revealed further that the immunoreactivity localized to the intermediate cells in the stria vascularis (Fig. 3A,B).

Intermediate cells abundantly express K^+ channels (Takeuchi and Ando, 1998, 1999), which may be important for K^+ transport in the stria vascularis and production of the endocochlear potential (Takeuchi et al., 2000). Basolateral membranes of marginal cells make a close contact with intermediate cells and heavily express ion transporters, such as Na^+,K^+-ATPase, the $Na^+,K^+,2Cl^-$ cotransporter, and Cl^- channels (Iwano et al., 1989; Crouch et al., 1997; Takeuchi and Irimajiri, 1996). Vigorous ion transport across plasma membranes of intermediate cells and marginal cells has been suggested (Iwano et al., 1989; Crouch et al., 1997; Takeuchi and Irimajiri, 1996). Since AQP1 immunoreactivity in the stria vascularis localizes to the region dense with ion transporters (Fig. 3), AQP1 may play a role in water distribution associated with vigorous ion transport in the stria vascularis.

Acknowledgements

We would like to thank Associate Prof. Taketoshi Taniguchi for his enthusiastic and expert help and Prof. Hiroshi Kimura and Prof. Ikuo Tooyama for their excellent technical advice.

References

Bagger-Sjöbäck, D., 1999. Possible role of the endolymphatic sac in the pathogenesis of Meniere's disease. In: Harris, J.P. (Ed.), Meniere's Disease. Kugler, The Hague, pp. 81–99.

Beitz, E., Kumagami, H., Krippeit-Drews, P. et al., 1999. Expression pattern of aquaporin water channels in the inner ear of the rat. The molecular basis for a water regulation system in the endolymphatic sac. Hear. Res. 132, 76–84.

Crouch, J.J., Sakaguchi, N., Lytle, C. et al., 1997. Immunohistochemical localization of the Na-K-Cl co-transporter (NKCC1) in the gerbil inner ear. J. Histochem. Cytochem. 45, 773–778.

Denker, B.M., Smith, B.L., Kuhajda, F.P. et al., 1988. Identification, purification, and partial characterization of a novel Mr 28,000 integral membrane protein from erythrocytes and renal tubules. J. Biol. Chem. 263, 15634–15642.

Hallpike, C., Cairns, H., 1938. Observation on the pathology of Meniere's syndrome. J. Laryngol. 53, 625–655.

Iwano, T., Yamamoto, A., Omori, K. et al., 1989. Quantitative immunocytochemical localization of Na^+,K^+-ATPase alpha-subunit in the lateral wall of rat cochlear duct. J. Histochem. Cytochem. 37, 353–363.

Kimura, R.S., 1967. Experimental blockage of the endolymphatic duct and sac and its effect on the inner ear of the guinea pig. A study on endolymphatic hydrops. Ann. Otol. Rhinol. Laryngol. 76, 664–687.

Schnermann, J., Chou, C.L., Ma, T. et al., 1998. Defective proximal tubular fluid reabsorption in transgenic aquaporin-1 null mice. Proc. Natl. Acad. Sci. USA 95, 9660–9664.

Stankovic, K.M., Adams, J.C., Brown, D., 1995. Immunolocalization of aquaporin CHIP in the guinea pig inner ear. Am. J. Physiol. 269, C1450–C1456.

Takeuchi, S., Ando, M., 1998. Inwardly rectifying K^+ currents in intermediate cells in the cochlea of gerbils: a possible contribution to the endocochlear potential. Neurosci. Lett. 247, 175–178.

Takeuchi, S., Ando, M., 1999. Voltage-dependent outward K^+ current in intermediate cell of stria vascularis of gerbil cochlea. Am. J. Physiol. 277, C91–C99.

Takeuchi, S., Irimajiri, A., 1996. A novel, volume-correlated Cl^- conductance in marginal cells dissociated from the stria vascularis of gerbils. J. Membr. Biol. 150, 47–62.

Takeuchi, S., Ando, M., Kozakura, K. et al., 1995. Ion channels in basolateral membrane of marginal cells dissociated from gerbil stria vascularis. Hear. Res. 83, 89–100.

Takeuchi, S., Ando, M., Kakigi, A., 2000. Mechanism generating endocochlear potential: role played by intermediate cells in stria vascularis. Biophys. J. 79, 2572–2582.

Takumi, Y., Nagelhus, E.A., Eidet, J. et al., 1998. Select types of supporting cell in the inner ear express aquaporin-4 water channel protein. Eur. J. Neurosci. 10, 3584–3595.

van Os, C.H., Kamsteeg, E.J., Marr, N. et al., 2000. Phsyiological relevance of aquaporins: luxury or necessity? Pflugers Arch. Eur. J. Physiol. 440, 513–520.

ELSEVIER

Auris Nasus Larynx 30 (2003) 349–354

AURIS NASUS LARYNX
INTERNATIONAL JOURNAL OF ORL & HNS

www.elsevier.com/locate/anl

Electrocochleographic findings in cases of autoimmune disease with sensorineural deafness

Akinobu Kakigi*, Shoichi Sawada, Taizo Takeda, Shunji Takeuchi, Kasumi Higashiyama, Hiroshi Azuma, Kazuhiro Yamakawa

Department of Otolaryngology, Kochi Medical School, Nankoku, Kochi 783-8505, Japan

Received 5 July 2001; accepted 18 July 2003

Abstract

Objectives: To present electrocochleographic findings in patients with autoimmune disease (AD) with sensorineural deafness (ADSD), and to discuss the etiologies of sensorineural hearing loss (SNHL) in cases of ADSD. *Methods:* Study design is a retrospective review of electrocochleographic results of 26 patients with ADSD. To evaluate the electrocochleographic results, average SP/AP ratios were compared between ADSD and normal subjects. In the ADSD group, audiologic pattern, fluctuations in hearing and results of the glycerol test were also reviewed. Electrocochleography (ECoG) was recorded using the extratympanic method, and the SP to AP ratio (SP/AP ratio) was analyzed. *Results:* The mean of average SP/AP ratios in the ADSD groups (0.46) was significantly higher than that in normal subjects (0.27). Further, 17 of 29 affected ears in patients with ADSD showed fluctuating hearing loss. Eighteen ears showed low tone loss (rising and peak audiologic patterns). Only 5 of 26 ears (19.2%) showed positive results on glycerol test. There was no correlation between glycerol test results and hearing fluctuation or between glycerol test results and the SP/AP ratio on χ^2-test. There was no tendency between audiologic pattern and glycerol test results or between audiologic pattern and the SP/AP ratio. *Conclusion:* These results suggest the etiologies of SNHL in cases of ADSD remain unclear. However, some cases showed clinical findings similar to endolymphatic hydrops. We should bear in mind that clinical Meniere's syndrome involves ADSD. Further investigation is needed to resolve the etiology of SNHL of ADSD.

Keywords: Electrocochleography; Autoimmune disease; Sensorineural hearing loss; Endolymphatic hydrops; Fluctuating hearing loss

1. Introduction

Autoimmune ear disease (AIED) was proposed as a new clinical entity by McCabe [1] AIED is characterized by several clinical outcomes. It is usually a bilateral disease, but may also by asymmetric. The hearing organs are always involved, and usually the balance organs are affected as well. Temporary facial paralysis may occur. Tissue destruction may occur and may involve the tympanic membrane, the entire middle ear, or the middle ear and mastoid. Sensorineural hearing loss (SNHL) may respond to immunosuppressive therapy. Recently, Western blot analysis of sera in patients with AIED demonstrated positive banding against inner ear antigens with molecular weights of 27–34, 45–50, 60, 65–68, 80, and 220 kDa [2–5]. Clinically, we often encounter a similar autoimmune-mediated SNHL associated with autoimmune disease (AD), e.g. aortitis syndrome [6,7], Behçet's disease [8–11], Cogan's disease [12,13], relapsing polychondritis [14,15], rheumatoid arthritis [16–18], Sjögren's syndrome [19,20], systemic lupus erythematosus [21–24], ulcerative colitis [25–27] and Wegener's granulomatosis [28–30]. The SNHL associated with AD may also be mediated by some inner ear antigens as well. In the present study, SNHL accompanied by AD is referred to as autoimmune disease with sensorineural deafness (ADSD).

Characteristic features of immune-mediated SNHL may be divided into three main types by the course of deafness, namely, sudden deafness, fluctuant hearing, and rapidly progressive SNHL [31]. A large number of clinical reports have described SNHL in cases of ADSD

* Corresponding author. Tel.: +81-88-880-2393; fax: +81-88-880-2395.

E-mail address: kakigia@kochi-ms.ac.jp (A. Kakigi).

0385-8146/03/$ - see front matter © 2003 Elsevier B.V. All rights reserved.
doi:10.1016/j.anl.2003.07.002

[6–30]. Most of the reports focused mainly on audiometric findings, but not on electrocochleographic findings. In the present study, we mainly present the results of electrocochleography (ECoG).

2. Materials and methods

Thirty-two ears of normal subjects and 29 of those with ADSD were investigated. Normal subjects were volunteers who showed normal hearing by pure tone audiometry and the absence of ear disease. The Departments of Internal Medicine or Dermatology at Kochi Medical School diagnosed as AD. Concerning the period of AD diagnosis, some patients were diagnosed before consulting our department; others were diagnosed after consulting our department.

All subjects except for the left ear of case 15 underwent ECoG and pure tone audiometry, which was performed before the ECoG recording. To obtain a good response, ECoG was basically recorded during a period of better hearing if the patient with autoimmune disease reported fluctuating hearing loss. All ECoG recordings were performed by the first and second authors using the extratympanic method. The equipment used for ECoG testing was a commercially available auditory evoked potential system (Nihon Koden, MEB-7102). The active electrode was a stainless needle covered with enamel, except at the tip. The needle electrode was placed on the posterosuperior wall of the external auditory meatus near the annulus. A reference electrode was placed on the ipsilateral mastoid process, and the ground electrode was placed on the forehead. Acoustic stimuli were alternating clicks produced by a square wave for 100 μs. The intensity of clicks was decreased in 10 dB steps from 90 dB nHL. The potentials were amplified and filtered using a band-pass at 8–3000 Hz. The sweep time was 10 ms following the onset of a click. ECoG recording was generally made only once, because this method is an invasive procedure, e.g. needle puncture on the external auditory meatal skin. To investigate the possible existence of endolymphatic hydrops, analysis of ECoG focused mainly on SP/AP ratios at the intensity of 90 dB nHL. For comparison of SP/AP ratios between ADSD and normal subjects, statistical analysis was conducted using Student's *t*-test. Fig. 1 shows the way of measuring the SP/AP ratio and a typical pattern of increase in the SP/AP ratio from a patient with ADSD.

In the ADSD group, fluctuations in hearing were investigated using pure tone audiometry, whereas some underwent a glycerol test. The criteria for fluctuation of hearing were as follows: the pure tone threshold shows both deprivation and improvement; the pure tone threshold changed in two octaves by at least 30 dB. For the glycerol test, a 50% glycerol solution was

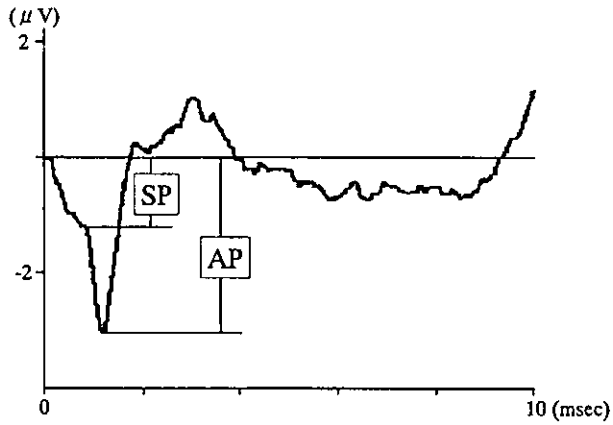

Fig. 1. Typical pattern of SP/AP ratio increase and SP/AP ratio measurement. This ECoG result is from case 6, left ear. The methods of measuring SP and AP are indicated and SP/AP ratio was 0.42. SP: summating potential; AP: action potential.

administered orally at a dose of 2.6 ml/kg of body weight. Pure tone audiometry was performed immediately before and 3 h after glycerol ingestion. The criteria for a positive glycerol test were defined as a pure tone threshold improvement of at least 10 dB in two adjacent octaves. A pure tone threshold improvement of 5–10 dB in three adjacent octaves was regarded as intermediate. The criteria for determining the effect of therapy were as follows. Hearing improvement after medication occurring two or more times after every treatment was regarded as effective. When only one treatment improved hearing and when the hearing did not change, such cases were also regarded as effective. We gave priority to medical treatment of autoimmune disease. For this reason, medical treatment for hearing loss was not given in all patients.

3. Results

Table 1 shows a summary of patients. The male:female ratio in ADSD was 2:14, showing a significant difference. Average patient age at the time of ECoG recordings was 56.3 years. Thirteen of 16 had bilateral SNHL. Seventeen of 29 affected ears showed fluctuating hearing loss. Eighteen ears showed low tone loss (rising and peak audiologic patterns). The mean follow-up period was 44.6 months (4–154 months). Glycerol test demonstrated positive results in 5 of 26 ears, intermediate results in 6 ears, and negative results in 13 ears. There was no correlation between glycerol test results and hearing fluctuation (Table 2) or between glycerol test results and the SP/AP ratio (Table 3) on χ^2-test. There was no correlatin between audiologic pattern and glycerol test results (Table 4) or between audiologic pattern and the SP/AP ratio (Table 5).

Table 1
Summary of ear disorders in 16 patients with autoimmune disease

Patient number	Age	Sex	Autoimmune disease	Affected ear	Audiologic pattern		Fluctuation of hearing	PTA at ECoG (dB)		Glycerol test		SP/AP		Vestibular symptom		Follow-up (month)	Effect of treatment	
					R	L		R	L	R	L	R	L	V	D		Immunosuppressive	Osmotic dehydration
1	31	Female	Behçet disease	Left		Rising	Left	2.5	36.3		−		0.50	−	+	70		
2	65	Female	Behçet disease	Bilateral	Peak	Falling	Non	36.3	41.3			0.99	0.70	−	+	16		
3	60	Female	Behçet disease	Bilateral	Peak	Peak	Bilateral	13.8	65	−	−	0.23	NR	−	+	154	+	
4	59	Female	Behçet disease	Left		Rising	Left	8.8	31.3		−		0.23	+	+	83	+	+
5	56	Female	ITP	Bilateral	Falling	Falling	Non	36.3	73.8	±	+	0.42	NR	+	+	25	−	−
6	38	Male	Malignant RA	Bilateral	Rising	Rising	Bilateral	50	12.5	±	±	0.46	0.42	+	+	36	−	+
7	64	Female	PSS	Bilateral	Rising	Falling	Right	31.3	30	+	−	0.42	0.35	−	+	48		−
8	70	Male	RA	Bilateral	Peak	Peak	Non	16.3	16.3	±	−	0.40	0.44	−	−	4		
9	61	Female	RA	Bilateral	Falling	Falling	Bilateral	11.3	11.3			0.77	0.54	−	+	39	−	
10	65	Female	Sarcoidosis	Bilateral	Peak	Peak	Bilateral	12.5	12.5	+	−	0.39	0.42	−	+	13		
11	61	Female	Sarcoidosis	Bilateral	Peak	Peak	Right	41.3	38.8	−	+	0.09	0.29	−	+	14	−	−
12	69	Female	Sjögren's syndrome	Bilateral	Flat	Flat	Bilateral	33.8	35	−	−	0.38	0.41	−	+	92		
13	70	Female	Sjögren's syndrome	Bilateral	Peak	Peak	Non	30	21.3	+	−	0.54	0.58	−	+	36		+
14	71	Female	Sjögren's syndrome	Left		Falling	Non	43.8	47.5				0.67	−	−	14		
15	40	Female	SLE	Bilateral	Flat	Flat	Bilateral	41.3	17.5	+	+	0.15		−	−	8		
16	29	Female	SLE	Bilateral	Rising	Rising	Left	8.8	8.8	−	−	0.56	0.58	−	−	62	−	

NR: no response; V: vertigo; D: dizziness.

Table 2
Comparison of glycerol test results and hearing fluctuation

Fluctuation	Glycerol test		
	Positive	Intermediate	Negative
Yes	3	3	9
No	2	3	4

There was no correlation between the glycerol test results and the presence of fluctuating hearing on χ^2-test.

Table 3
Comparison of the glycerol test results and SP/AP

SP/AP	Glycerol test		
	Positive	Intermediate	Negative
<0.4	2	1	5
≥ 0.4	1	5	7

There was no correlation between the glycerol test results and increments of SP/AP on χ^2-test.

Table 4
Comparison of audiologic pattern and glycerol test

Glycerol test	Audiologic pattern			
	Flat	Falling	Rising	Peak
Positive	2	1	1	1
Intermediate	0	2	2	3
Negative	2	0	4	6

There was no correlation between audiologic pattern and glycerol test results.

Table 5
Comparison of audiologic pattern and SP/AP

SP/AP	Audiologic pattern			
	Flat	Falling	Rising	Peak
<0.4	2	1	1	4
≥ 0.4	1	5	6	6

There was no correlation between audiologic pattern and the SP/AP ratio.

The average SP/AP ratios were compared between ADSD and normal hearing groups (Table 6). The SP/AP ratio increased significantly in patients with ADSD compared to that in the normal hearing group using Student's t-test.

4. Discussion

In the present study, 17 of 29 affected ears showed fluctuating hearing loss. Twelve of 16 cases showed vestibular symptoms (Table 1). The average SP/AP ratio in patients with ADSD was significantly higher than that in the normal hearing group. The results in this study were similar to those of patents with endolymphatic hydrops because fluctuating hearing loss, vestibular symptoms and increments of the SP/AP ratio are clinically characteristic findings of endolymphatic hydrops.

Table 6
Comparison of SP/AP in ears with autoimmune disease and normal hearing

	Autoimmune disease ($n=26$)	Normal hearing ($n=32$)
SP/AP	0.46 ± 0.19	0.27 ± 0.12^a

There was a significant difference between normal hearing and hearing loss in ears with autoimmune disease. Student's t-test was used to evaluate the difference in mean values between groups. P-values below 0.05 were considered significant. Note that 2 of 29 affected ears with autoimmune disease showed no response (see Table 1) and that one ear (case 15, left ear) did not undergo ECoG; n: number of ears.
[a] Significant difference from ears with autoimmune disease, $P < 0.05$. Results are expressed as means $\pm$ S.D.

Morphologically, Schuknecht and Nadol [32] reported that the following pathologic features characterize autoimmune inner ear disease with Cogan's syndrome: acute labyrinthitis resulting in atrophy of inner ear tissues including the sense organs and their supporting structures; endolymphatic hydrops; focal and diffuse proliferation of fibrous tissue and bone; and retrograde neuronal degeneration. Hoistad et al. [33] reported histopathologic findings in SNHL of autoimmune origin that included: organs of Corti missing or absent in all cochlear turns; cells decreased in spiral ganglia, and lymphocytic infiltration; absence of portions of the spiral prominence; endolymphatic hydrops in basal, middle, and apical cochlear turns and in the saccule and utricle; fibrosis and osteoneogenesis of a scala tympani of the basal turn of the cochlea, the posterior semicircular canal, and the canal of Cotugno; fibrosis of the vestibular aqueduct and endolymphatic sac; and lymphocytes in the endolymphatic sac, perisaccular area, inferior cochlear vein, and Rosenthal's canal. Since human temporal bone studies demonstrated endolymphatic hydrops in autoimmune ear disease, endolymphatic hydrops, which appears to be induced by AD, may have been one of the causes of SNHL of ADSD in this study. Lunardi et al. [34] demonstrated autoantibodies from Cogan's syndrome that are able to induce tissue damage on binding of cell-surface molecules present on the sensory epithelia of the inner ear and on endothelial cells. This mechanism of tissue damage might occur in cases of ADSD.

The glycerol test is also one of the tests for detecting endolymphatic hydrops. In our present study, only 5 of 26 ears (19.2%) showed a positive result on glycerol test.

This low proportion of positive results suggests that the etiology of SNHL in cases of ADSD involves not only endolymphatic hydrops but also irreversible damage to the inner ear, cochlear nerve and/or the endolymphatic sac. In other words, the etiology should be considered multiple including vasculitis, as McCabe [1] and human histopathological studies indicated [32,33]. Sone et al. [35] reported histopathologic findings in SNHL of SLE. They indicated that only 1 of 14 temporal bones showed endolymphatic hydrops. Rauch et al. [36] reported that there was not a strict and full correlation between endolymphatic hydrops and Meniere's-like symptom on human temporal bone pathology. The low number of positive results on the glycerol test seems to be consistent with their findings. Further, there were no correlations among audiologic patterns, fluctuations of hearing, ECoG and glycerol tests. These results also suggest variability in the etiology of ADSD.

The cases in this study received immunosuppressive therapy using prednisolone and cyclophosphamide and/or osmotic dehydration therapy by isosorbide to improve their hearing (Table 1). Treatment responses showed great variation. The lesions may be reversible in some cases because 17 of 29 ears (58.6%) showed fluctuating hearing loss. Therefore, therapy should be initiated before inner ear damage becomes irreversible. Actually, some patients showed improved hearing, while others developed progressive hearing loss despite treatment or showed no change in their hearing. Hearing loss, that responds to immunosupression and osmotic dehydration therapy may be caused by AIED and endolymphatic hydrops, respectively. However, there remain some cases of therapy-resistant hearing loss. Therefore, the cause of SNHL in patients with AD remains unclear. Further investigation is needed to resolve the etiology of SNHL of ADSD, e.g. Western blot and other serological studies.

5. Conclusion

Sixteen patients with AD had SNHL. Seventeen of 29 affected ears showed fluctuating hearing loss. Eighteen ears showed low tone loss (rising and peak audiologic patterns). ECoG results showed increments of SP/AP, that were significantly larger than those in the normal hearing group. These results are similar to clinical findings in patients with endolymphatic hydrops. However, only 5 of 26 ears (19.2%) showed a positive result on glycerol test. This low proportion of positive results implies that the etiology of SNHL in individuals with ADSD is not limited to endolymphatic hydrops, but also involves other causes. Physicians should be aware that clinical Meniere's syndrome may include ADSD.

References

[1] McCabe BF. Autoimmune sensorineural hearing loss. Ann Otol Rhinol Laryngol 1979;88:585–9.
[2] Veldman JE, Hanada T, Meeuwsen F. Diagnostic and therapeutic dilemmas in rapidly progressive sensorineural hearing loss and sudden deafness. Acta Otolaryngol (Stockh) 1993;113:303–6.
[3] Yamanobe S, Harris JP. Inner ear-specific autoantibodies. Laryngoscope 1993;103:319–25.
[4] Mosciscki RA, San Martin JE, Quintero C, Rauch SD, Nadol JB, Bloch KJ. Serum antibody to inner ear proteins in patients with progressive hearing loss. JAMA 1994;272:611–6.
[5] Cao MY, Deggouj N, Gersdorff M, Tomasi J-P. Guinea pig inner ear antigens: extraction and application to the study of human autoimmune inner ear disease. Laryngoscope 1996;106:207–12.
[6] Siglock TJ, Brookler KH. Sensorineural hearing loss associated with Takayasu's disease. Laryngoscope 1987;97:797–800.
[7] Kunihiro T, Kanzaki J, O-Uchi T, Yoshida A. Steroid-responsive sensorineural hearing loss associated with aortitis syndrome. ORL 1990;52:86–95.
[8] Andreoli C, Savastano M. Audiologic pathology in Behcet syndrome. Am J Otol 1989;10:466–7.
[9] Smith LN. Unilateral sensorineural hearing loss in Behcet's disease. Am J Otolaryngol 1994;15:286–8.
[10] Igarashi Y, Watanabe Y, Aso S. A case of Behcet's disease with otologic symptoms. ORL 1994;56:295–8.
[11] Soylu L, Aydogan B, Soylu M, Ozsahinoglu C. Hearing loss in Behcet's disease. Ann Otol Rhinol Laryngol 1995;104:864–7.
[12] Cogan DG. Syndrome of nonsyphilitic interstitial keratitis and vestibuloauditory symptoms. Arch Ophthalmol 1945;33:144–9.
[13] Norton EWD, Cogan DG. Syndrome of nonsyphilitic interstitial keratitis and vestibuloauditory symptoms. Arch Ophthalmol 1959;61:695–7.
[14] McCaffrey TV, McDonald TJ, McCaffrey LA. Head and neck manifestations of relapsing polychondritis: review of 29 cases. ORL 1978;86:473–8.
[15] Kimura Y, Miwa H, Furukawa M, Mizukami Y. Relapsing polychondritis presented as inner ear involvement. J Laryngol Otol 1996;110:154–7.
[16] Kastanioudakis I, Skevas A, Danielidis V, Tsiakou E, Drosos AA, Moustopoulos MH. Inner ear involvement in rheumatoid arthritis: a prospective clinical study. J Laryngol Otol 1995;109:713–8.
[17] Magaro M, Zoli A, Altomonte L, Mirone L, Corvino G, Di Girolamo S, Giacomini P, Alessandrini M. Sensorineural hearing loss in rheumatoid arthritis. Clin Exp Rheumatol 1990;8:487–90.
[18] Elwany S, el Garf A, Kamel T. Hearing and middle ear function in rheumatoid arthritis. J Rheumatol 1986;13:878–81.
[19] Newton VE. Sensorineural hearing loss and the Marinesco-Sjogren syndrome. J Laryngol Otol 1991;105:210–2.
[20] Tumiati B, Casoli P, Parmeggiani A. Hearing loss in the Sjogren syndrome. Ann Intern Med 1997;126:450–3.
[21] Bowman CA, Linthicum FH, Jr., Nelson RA, Mikami K, Quismorio F. Sensorineural hearing loss associated with systemic lupus erythematosus. Otolaryngol Head Neck Surg 1986;94:197–204.
[22] Caldarelli DD, Rejowski JE, Corey JP. Sensorineural hearing loss in lupus erythematosus. Am J Otol 1986;7:210–3.
[23] Kobayashi S, Fujishiro N, Sugiyama K. Systemic lupus erythematosus with sensorineural hearing loss and improvement after plasmapheresis using the double filtration method. Intern Med 1992;31:778–81.
[24] Kataoka H, Takeda T, Nakatani H, Saito H. Sensorineural hearing loss of suspected autoimmune etiology: a report of three cases. Auris Nasus Larynx 1995;22:53–8.

[25] Summers RW, Harker L. Ulcerative colitis and sensorineural hearing loss: is there a relationship? J Clin Gastroenterol 1982;4:251–2.
[26] Weber RS, Jenkins HA, Coker NJ. Sensorineural hearing loss associated with ulcerative colitis. A case report. Arch Otolaryngol 1984;110:810–2.
[27] Kumar BN, Walsh RM, Wilson PS, Carlin WV. Sensorineural hearing loss and ulcerative colitis. J Laryngol Otol 1997;111:277–8.
[28] McCaffrey TV, McDonald TJ, Facer GW, DeRemee RA. Otologic manifestations of Wegener's granulomatosis. Otolaryngol Head Neck Surg 1980;88:586–93.
[29] Dwyer J, Janzen VD. Wegener's granulomatosis with otological and nervous system involvement. J Otolaryngol 1981;10:476–80.
[30] Clements MR, Mistry CD, Keith AO, Ramsden RT. Recovery from sensorineural deafness in Wegener's granulomatosis. J Laryngol Otol 1989;103:515–8.
[31] Veldman J. Immune-mediated sensorineural hearing loss. Auris Nasus Larynx 1998;25:309–17.
[32] Schuknecht HF, Nadol JB. Temporal bone pathology in a case of Cogan's syndrome. Laryngoscope 1994;104:1135–43.
[33] Hoistad DL, Schachern PA, Paparella MM. Autoimmune sensorineural hearing loss: a human temporal bone study. Am J Otolaryngol 1998;19:33–9.
[34] Lunardi C, Bason C, Leandri M, Navone R, Lestani M, Millo E, Benatti U, Cilli M, Beri R, Corrocher R, Puccetti A. Autoantibodies to inner ear and endothelial antigens in Cogan's syndrome. Lancet 2002;360:915–21.
[35] Sone M, Schachern PA, Paparella MM, Morizono N. Study of systemic lupus erythematosus in temporal bones. Ann Otol Rhinol Laryngol 1999;108:338–44.
[36] Rauch SD, Merchant SN, Thedinger BA. Meniere's syndrome and endolymphatic hydrops. Double-blind temporal bone study. Ann Otol Rhinol Laryngol 1989;98:873–83.

Acta Otolaryngol 2004; 124: 1046–1052

Taylor & Francis
healthsciences

Vertical Canal Function in Normal Subjects and Patients with Benign Paroxysmal Positional Vertigo

KAZUNORI SEKINE[1], TAKAO IMAI[2], MASAHIRO MORITA[2], KOJI NAKAMAE[3], KATSUYOSHI MIURA[3], HIROMU FUJIOKA[3], TAKESHI KUBO[2], KOICHI TAMURA[1] and NORIAKI TAKEDA[1]

From the [1]Department of Otolaryngology, University of Tokushima School of Medicine, Tokushima, Japan, [2]Department of Otolaryngology and Sensory Organ Surgery, Osaka University Graduate School of Medicine, Osaka, Japan and [3]Department of Information Systems Engineering, Osaka University Graduate School of Engineering, Osaka, Japan

Sekine K, Imai T, Morita M, Nakamae K, Miura K, Fujioka H, Kubo T, Tamura K, Takeda N. *Vertical canal function in normal subjects and patients with benign paroxysmal positional vertigo.* Acta Otolaryngol 2004; 124: 1046–1052.

Objectives—To assess the dynamics of the vertical semicircular canal (VSCC)-ocular reflex in normal subjects and then to compare their gain in VSCC-ocular reflex with that of patients with benign paroxysmal positional vertigo (BPPV).

Material and Methods—Subjects were sinusoidally rotated around the earth-vertical axis with their head tilted 60° backward and turned 45° to the right or left side from the sagittal plane at frequencies of 0.1, 0.3, 0.5, 0.7 and 1.0 Hz with a maximum angular velocity of 50°/s. Head rotation to the right side on the right anterior semicircular canal (SCC)–left posterior SCC plane or to the left side on the left anterior SCC–right posterior SCC plane stimulated the pair of VSCCs. Eye movements were recorded on a video imaging system with an infrared charge-coupled device camera, using our new technique for analyzing the rotation vector of eye movements in three dimensions.

Results—The mean gains in left posterior SCC-ocular reflex in normal subjects ranged from 0.44 at 0.1 Hz to 0.79 at 1.0 Hz, while the mean gains in right anterior SCC-ocular reflex ranged from 0.45 at 0.1 Hz to 0.73 at 1.0 Hz. The mean gains in right posterior SCC-ocular reflex in normal subjects ranged from 0.53 at 0.1 Hz to 0.89 at 1.0 Hz, while the mean gains in left anterior SCC-ocular reflex ranged from 0.53 at 0.1 Hz to 0.88 at 1.0 Hz. Thus, the gains in VSCC-ocular reflex did not differ among the four VSCCs in normal subjects. Similarly, vestibulo-ocular reflex (VOR) gains of the four VSCCs in patients with right- or left-sided BPPV were almost the same at all frequencies compared to those of normal subjects.

Conclusion—In patients with BPPV, gains in VOR in the four VSCCs were not changed in comparison with those of normal subjects. It is suggested that the mass of free-floating otoconial debris associated with canalolithiasis was too small compared to that of the endolymph to change the canal dynamics. *Key words: benign paroxysmal positional vertigo, rotation test, vertical semicircular canal.*

INTRODUCTION

The conventional clinical tests of semicircular canal function are the caloric and rotation tests, which evaluate the function of the lateral semicircular canal (LSCC). Recently, we developed a new rotatory chair for testing vertical semicircular canal (VSCC) function (1, 2) and reported that the angular velocity of post-rotatory nystagmus induced by the VSCC is weaker than that induced by the LSCC (3). As previously reported by Decher (4), our result also suggested lower sensitivity of the VSCC compared to the LSCC. However, the possibility cannot be excluded that the reduced sensitivity of the VSCC was due to the fact that we only analyzed the vertical component of post-rotatory nystagmus induced by the VSCC, which in fact consists of both vertical and torsional components.

In order to calculate the exact gain in VSCC-ocular reflex, which is the ratio of the compensatory eye velocity around the rotation axis to head velocity, the rotation vector but not the Fick coordinates of eye movements should be analyzed. For this purpose, we have developed a new video imaging technique for analyzing the 3D rotation vector of eye movements (5). In the present study, using our new rotatory chair and video imaging technique, we assessed the dynamics of the VSCC-ocular reflex in normal subjects. We then compared the gain in VSCC-ocular reflex in normal subjects with that of patients with benign paroxysmal positional vertigo (BPPV), whose lesion is supposed to be in the posterior semicircular canal (SCC).

MATERIAL AND METHODS

Subjects

The study subjects comprised 8 normal healthy volunteers (3 males, 5 females; age range 23–32 years; mean age 26.1 ± 2.8 years) with no history of neuro-otological disease and 11 patients with BPPV. In patients with BPPV, the right posterior SCC was affected in 6 patients (R-BPPV; 3 males, 3 females; age range 38–75 years; mean age 63.5 ± 14.2 years) and the left posterior SCC was affected in 5 (L-BPPV; 3 males, 2 females; age range 29–84 years; mean age 51.2 ± 22.5 years).

BPPV was diagnosed by means of the following criteria:

 ISSN 0001-6489

DOI 10.1080/00016480410018061

1. Absence of an identifiable central nervous system disorder able to explain the positional vertigo on both neurological examination and neuroradiological studies of the brain.
2. No spontaneous nystagmus.
3. History of brief episodes of positional vertigo.
4. A positive response to the Dix–Hallpike maneuver of vertical-beating nystagmus and a torsional component that was either counterclockwise on head hanging right (diagnosis of R-BPPV) or clockwise on head hanging left (diagnosis of L-BPPV).
5. Nystagmus showing a short latency after head hanging and lasting for up to 60 s.

This study was performed in accordance with guidelines approved by the Committee for Medical Ethics of the University of Tokushima School of Medicine and an informed consent form was obtained from each subject prior to the rotation test.

Experimental protocols

Subjects were seated on a computer-controlled rotating chair with their head tilted 60° backward and turned 45° to the right or left side from the sagittal plane in order to stimulate the VSCCs. The VSCCs are aligned diagonally in the head and form two approximately co-planar pairs: the right anterior SCC/left posterior SCC (RALP) pair and the left anterior SCC/right posterior SCC (LARP) pair. Consequently, the RALP (Fig. 1a) or LARP planes (Fig. 1b) were brought into a plane perpendicular to the rotational axis of the chair, and each pair of VSCCs was periodically stimulated (6–8). Clockwise rotation on the RALP plane stimulates the left posterior SCC by ampullofugal endolymphatic flow and partly inhibits the right anterior SCC by ampullopetal endolymphatic flow. In this condition, we used the angular eye velocity of per-rotatory nystagmus around the eye rotation axis as an index of left posterior SCC function. For counterclockwise rotation on the RALP plane, the angular eye velocity of per-rotatory nystagmus around the eye rotation axis was an index of right anterior SCC function. For clockwise or counterclockwise rotation on the LARP plane, the angular eye velocity of per-rotatory nystagmus around the eye rotation axis was an index of right posterior or left anterior SCC function, respectively. The center of the head was aligned with the chair rotational axis so that linear acceleration during the rotation was minimal (1–3). Subjects were sinusoidally rotated with eyes open in complete darkness at frequencies of 0.1, 0.3, 0.5, 0.7 and 1.0 Hz with a maximum angular velocity of 50°/s. To stay alert during rotation, subjects were asked to perform mental arithmetic during the whole

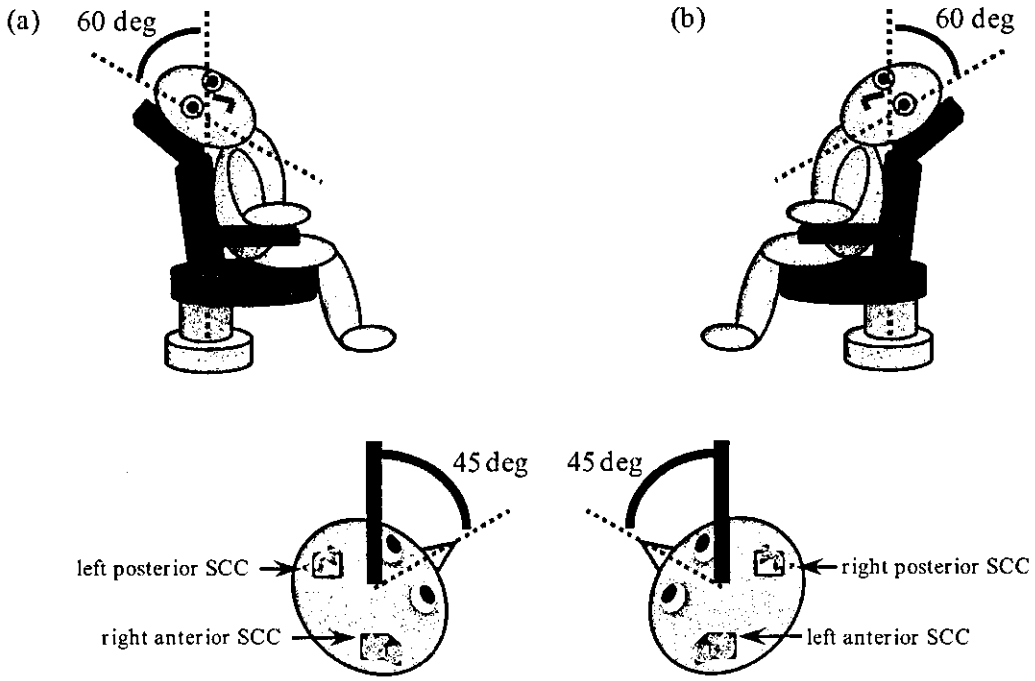

Fig. 1. Subjects with their head tilted 60° backward and turned 45° to the right side were sinusoidally rotated on the RALP plane to stimulate the right anterior and left posterior SCCs (a), whereas subjects with their head tilted 60° backward and turned 45° to the left side were sinusoidally rotated on the LARP plane to stimulate the left anterior and right posterior SCCs (b).

procedure. The interval between the rotational tests at different rotation frequencies was ≈ 5 min.

Recording system and data analysis

Eye movements were recorded as digital images (resolution 720 × 480) using an infrared charge-coupled device (CCD) camera trained on the left eye. The sampling rate of digital images was 30 Hz, the center of eye rotation on the image plane was determined as a point and the radius of the eyeballs was calculated. The center of the pupil and an iris freckle at each digital image were also determined as the point on the image plane. The point of the center of pupil and an iris freckle on the image plane were calculated to the 3D head coordinates of the center of pupil and an iris freckle, determined by the point of the center of eye rotation on the image plane and radius of eyeball. The rotation vectors of the 3D eye position were calculated from the head coordinates of the center of the pupil and an iris freckle. Furthermore, to calculate the exact gain in vestibulo-ocular reflex (VOR), which is the ratio of the compensatory eye velocity around the rotation axis to head velocity, the rotation vector but not Fick coordinates of the eye movements must be analyzed. Accordingly, the eye velocity around the rotation axis was derived from the rotation vectors of the eye position. The method of analysis of eye rotation vectors has been described elsewhere (5). We calculated eye velocities around the rotation axis as the magnitude of the rotation vector that represents the velocity. These values were positive when unrelated to the direction of eye rotation. To express eye velocities around the rotation axis, a right-handed rule was chosen and the mark of the velocities around the rotation was synchronized to that of the Z component, the largest of all components. Fast eye movements were removed to give cumulative slow-phase eye velocities. After synchronizing the mark and removing fast eye movements, eye velocities were approximated by the best-fitted sine curve in each right- and leftward eye movement using the least-squares method (9). The frontal gaze eye position was chosen as the reference point. Head coordinates (X, Y, Z) were also defined using the right-handed rule, so that the X axis was parallel to the naso-occipital axis (positive forward), the Y axis parallel to the inter-aural axis (positive left) and the Z axis normal to the X–Y plane (positive upwards).

We determined the maximum slow-phase eye velocity (MSPV) on rotation to the right and left sides around the rotation axis from the best-fitted sine curve, and the gain in VOR was calculated as the ratio of the MSPV to the maximum head angular velocity (50°/s).

Statistical analysis

Changes in VOR gain were tested using repeated-measures ANOVA. Further comparisons at each frequency were analyzed by means of Bonferroni/Dunn's test and $p < 0.05$ was considered significant.

RESULTS

Figure 2 shows the 3D angular eye velocities of per-rotatory nystagmus in a normal subject on rotation on the (a) RALP and (b) LARP planes at frequencies of (A) 0.1, (B) 0.5 and (C) 1.0 Hz. Figure 3 shows the angular eye velocities of per-rotatory nystagmus around the eye rotation axis in a normal subject on rotation on the (a) RALP and (b) LARP planes.

Figure 4 shows the frequency–response characteristics of the four VSCCs in normal subjects. In the RALP plane, the mean gains in the left posterior SCC-ocular reflex in normal subjects were 0.44 at 0.1 Hz, 0.49 at 0.3 Hz, 0.60 at 0.5 Hz, 0.66 at 0.7 Hz and 0.79 at 1.0 Hz, while the mean gains in the right anterior SCC-ocular reflex were 0.45 at 0.1 Hz, 0.48 at 0.3 Hz, 0.56 at 0.5 Hz, 0.63 at 0.7 Hz and 0.73 at 1.0 Hz. In the LARP plane, the mean gains in the right posterior SCC-ocular reflex in normal subjects were 0.53 at 0.1 Hz, 0.61 at 0.3 Hz, 0.62 at 0.5 Hz, 0.74 at 0.7 Hz and 0.89 at 1.0 Hz, while the mean gains in the left anterior SCC-ocular reflex were 0.53 at 0.1 Hz, 0.62 at 0.3 Hz, 0.65 at 0.5 Hz, 0.73 at 0.7 Hz and 0.88 at 1.0 Hz. Thus, the gains in the VSCC-ocular reflex did not differ significantly among the four VSCCs in normal subjects.

Figure 5a shows the frequency–response characteristics of the four VSCCs in patients with R-BPPV. In the RALP plane, the mean gains in the left posterior SCC-ocular reflex were 0.48 at 0.1 Hz, 0.49 at 0.3 Hz, 0.58 at 0.5 Hz, 0.59 at 0.7 Hz and 0.79 at 1.0 Hz, while the mean gains in the right anterior SCC-ocular reflex were 0.46 at 0.1 Hz, 0.47 at 0.3 Hz, 0.55 at 0.5 Hz, 0.58 at 0.7 Hz and 0.79 at 1.0 Hz. In the LARP plane, the mean gains in the right posterior SCC-ocular reflex were 0.41 at 0.1 Hz, 0.46 at 0.3 Hz, 0.60 at 0.5 Hz, 0.65 at 0.7 Hz and 0.83 at 1.0 Hz, while the mean gains for the left anterior SCC-ocular reflex were 0.42 at 0.1 Hz, 0.48 at 0.3 Hz, 0.61 at 0.5 Hz, 0.62 at 0.7 Hz and 0.82 at 1.0 Hz.

Figure 5b shows the frequency–response characteristics for the four VSCCs in patients with L-BPPV. The mean gains in the left posterior SCC-ocular reflex were 0.41 at 0.1 Hz, 0.55 at 0.3 Hz, 0.58 at 0.5 Hz, 0.71 at 0.7 Hz and 0.78 at 1.0 Hz, while the mean gains in the right anterior SCC-ocular reflex were 0.40 at 0.1 Hz, 0.52 at 0.3 Hz, 0.55 at 0.5 Hz, 0.67 at 0.7 Hz and 0.77 at 1.0 Hz. The mean gains in the right posterior SCC-ocular reflex were 0.48 at 0.1 Hz, 0.70

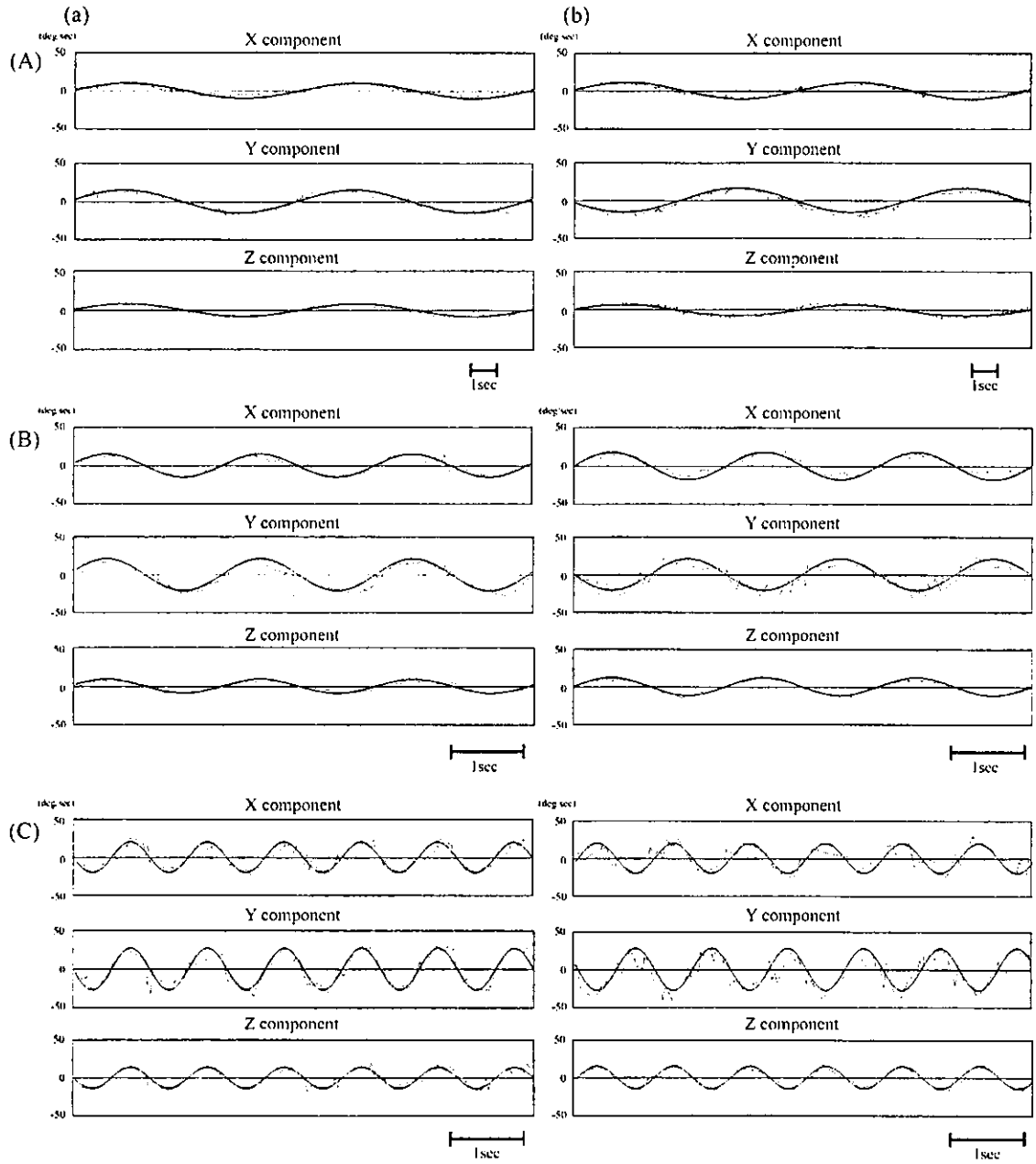

Fig. 2. X, Y and Z components of angular eye velocities of per-rotatory nystagmus in a normal subject for rotations on the (a) RALP and (b) LARP planes. (A) 0.1 Hz, (B) 0.5 Hz, (C) 1.0 Hz.

at 0.3 Hz, 0.76 at 0.5 Hz, 0.83 at 0.7 Hz and 0.84 at 1.0 Hz, while the mean gains for the left anterior SCC-ocular reflex were 0.46 at 0.1 Hz, 0.67 at 0.3 Hz, 0.71 at 0.5 Hz, 0.77 at 0.7 Hz and 0.80 at 1.0 Hz. Thus, VOR gains in the four VSCCs in patients with R- or L-BPPV were almost the same at all frequencies. These findings indicate that the gains in VSCC-ocular reflex in patients with BPPV were not significantly different from those of normal subjects at all frequencies.

DISCUSSION

The aim of this study was to assess the function of the VSCCs and compare their dynamics in normal subjects with those in patients with BPPV. In normal subjects, the mean gain in VOR in the four VSCCs ranged from 0.44 at 0.1 Hz to 0.79 at 1.0 Hz. At frequencies of 0.1–1.0 Hz, there were no significant differences in VOR gains in each VSCC in normal subjects. Moreover, at frequencies of 0.1–1.0 Hz, no significant differences were noticed in VOR gains in

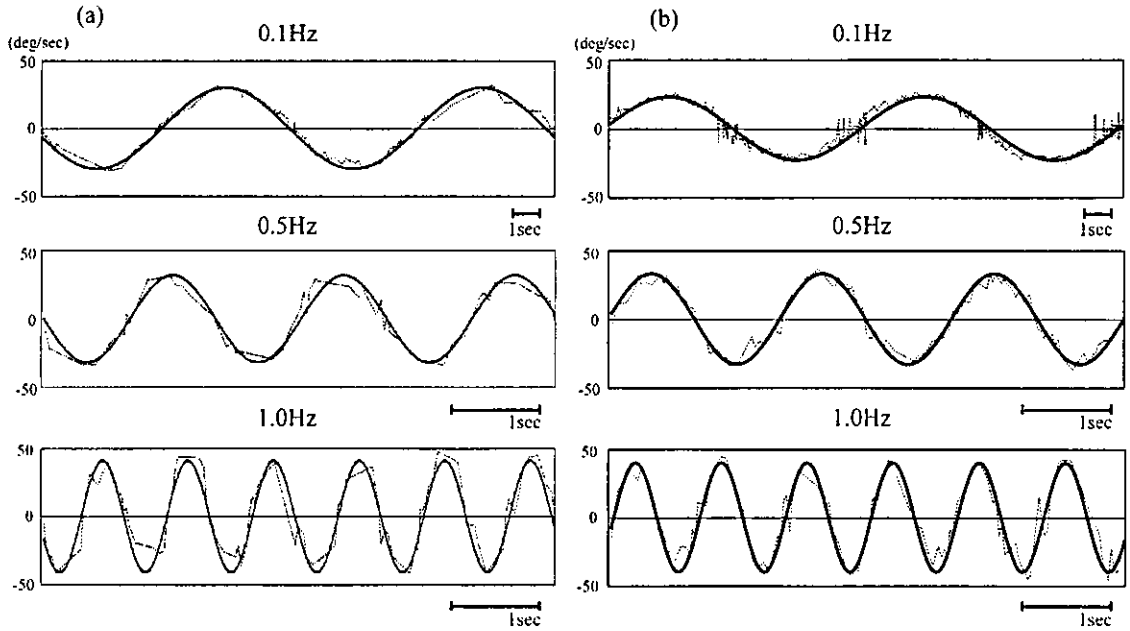

Fig. 3. Angular eye velocities of per-rotatory nystagmus around the rotation axis in a normal subject for rotations on the (a) RALP and (b) LARP planes.

each VSCC in normal subjects compared to those in patients with BPPV.

To assess the function of the VSCCs, we first developed a new rotation chair to stimulate them. Interestingly, Morita et al. (3) reported that the mean values of MSPV in both anterior and posterior SCC-induced post-rotatory nystagmus were lower than those induced by the LSCC, suggesting that the threshold to the angular velocity in the VSCC was lower than that in the LSCC. However, there is a possibility that the reduction of the VSCC-induced post-rotatory nystagmus was caused by analyzing only vertical components. As VSCC-induced nystagmus consists of three components in fixed head coordinates, each component changes its value at different head positions (10). To overcome this problem, we undertook a vector analysis of eye movements, because the eye velocity vector of VSCC-induced nystagmus is a more accurate index of VSCC function. Recently, we developed a new imaging technique to

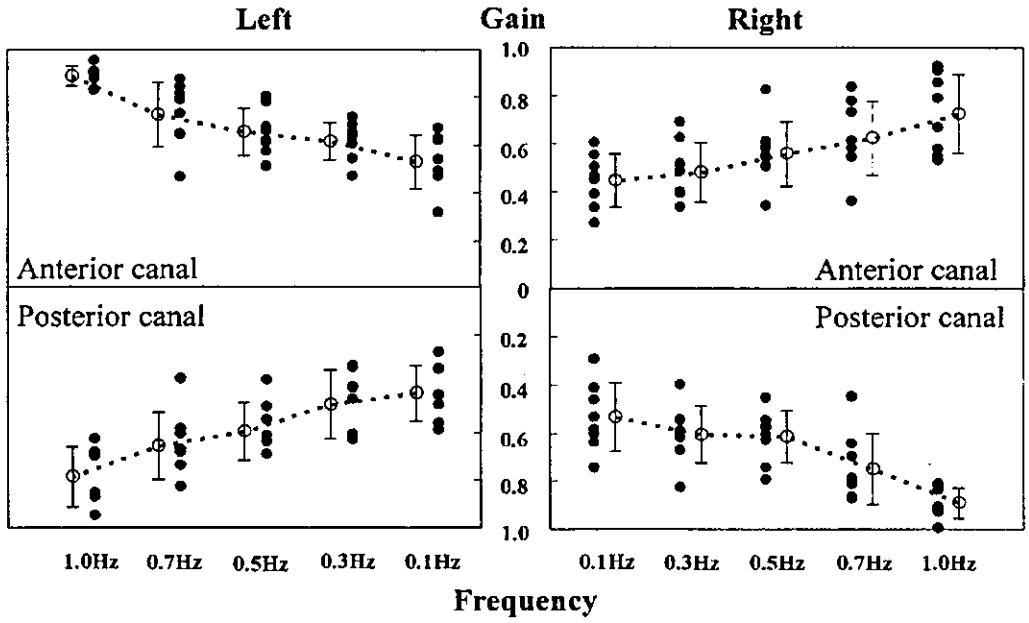

Fig. 4. Dynamics of the vertical VOR in the four VSCCs in a normal subject.

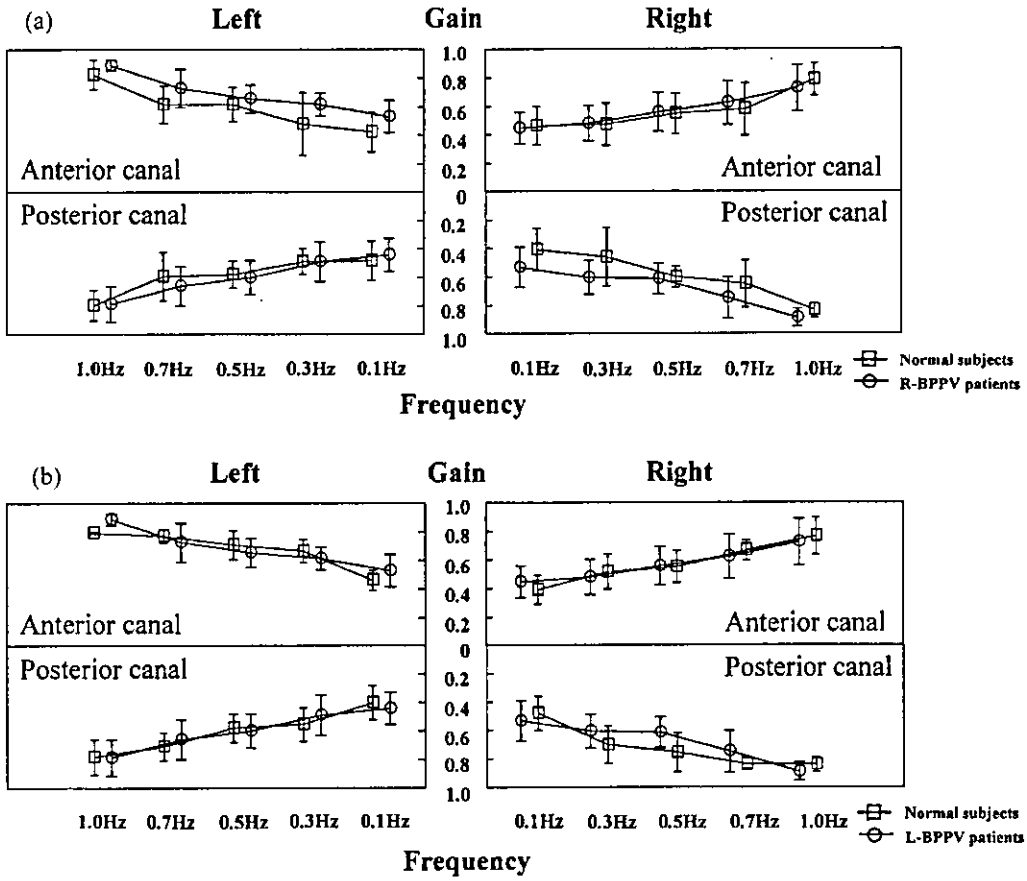

Fig. 5. Dynamics of the vertical VOR in the four VSCCs in patients with (a) R-BPPV and (b) L-BPPV.

analyze the rotation vector of eye movements in three dimensions using an infrared CCD camera (5). In order to evaluate the exact gain in the VSCC-ocular reflex, we measured the angular eye velocity of per-rotatory nystagmus around the eye rotation axis in the present study. Accordingly, the VOR gain in the VSCCs around the rotation axis was smaller than that in the LSCC in comparison with previous studies (11–14). Fetter et al. (10) and Tweed et al. (15) showed a lower torsional component in VOR gain compared to the yaw and pitch components. As the VOR gains of the VSCCs around the rotation axis consist of three components (Fig. 2), it is suggested that the lower torsional component caused the VOR gain of the VSCCs to be smaller than that of the LSCC.

It has already been shown (11–14) that the gain in the LSCC increases with the rotational frequency. Similarly, we also found that the VOR gain in the VSCC increased with the rotational frequency (Fig. 4). It is suggested that the cupula of the VSCC has the same dumping characteristics as that of the LSCC.

In patients with BPPV, Iida et al. (16) used the vertical component of the VSCC-ocular reflex and reported a significant reduction in the VOR gain of the affected posterior VSCC in comparison with those of other VSCCs. In the present study, we showed that the gains in VOR of the four VSCCs around the rotation axis in patients with BPPV were almost the same at all frequencies and that the gains in VOR that stimulated the four VSCCs in patients with BPPV were not significantly different from those of normal subjects at all frequencies (Figs 5a and 5b). Based on the canalolithiasis hypothesis of BPPV, free-floating otoconial debris in the SCC acts like a plunger, causing movement of the endolymph during changes in head position (17, 18). Because all patients in this study were cured after Eply's maneuver, which is based on the canalolithiasis hypothesis (17), it is suggested that they have canalolithiasis in the posterior SCC. In our previous study concerning the LSCC variant of BPPV (19), VOR gain of the LSCC at low frequency was reduced by cupulolithiasis, but not by canalolithiasis. Therefore, it is suggested that the mass of free-floating otoconial debris associated with canalolithiasis is too small compared to the mass of the endolymph to change the canal dynamics, as in the case of canalolithiasis in the LSCC (19).